Electronic Supporting Information

Ethyl Cellulose and Cetrimonium Bromide Assisted Synthesis of Mesoporous, Hexagon Shaped ZnO Nanodisks with Exposed ±{0001} Polar Facets for Enhanced Photovoltaic Performance in Quantum Dot Sensitized Solar Cells

Tridip Ranjan Chetia,[†] Mohammad Shaad Ansari,[†] and Mohammad Qureshi[*,†]*

[†]Materials Science Laboratory, Department of Chemistry, Indian Institute of Technology Guwahati, Guwahati–781039, Assam, India; *Corresponding Author email: mq@iitg.ernet.in

1. **Table S1**: An overview of the present Scenario of **ZnO Based CdS/CdSe co-sensitized** solar cells and their relevant performance parameters along with photovoltaics discussed in our manuscript

Ref No.	ZnO Nanostructures	J_{sc} (mA/cm^2)	V_{oc} (mV)	*FF* (%)	η (%)	Active Area (cm^2)	Counter electrode
8	ZnO NP	10.48	683	62.3	4.46	0.15	Cu_2S/brass foil
10	ZnO NW	17.30	627	38.3	4.15	0.25	Au/FTO
11	ZnO NW	12.60	685	42	3.60	0.25	*MSU-F-C/FTO
12	ZnO NW	5.19	661	41.5	1.42	No data	Pt/FTO
15	Tetrapod like ZnONP	13.85	722	42.4	4.24	0.25	Pt/FTO
18	ZnO NP and ZnO MS	17.13	560	53	5.08	No data	Cu_2S/brass foil
53	ZnO NR-ZnO NS	10.74	610	50	3.28	0.25	Cu_2S/brass foil
SI 1	ZnO NP (Surface passivated with TiO_2 shell)	15.4	620	49	4.7	0.25	Cu_2S/brass foil
Present work	**ZnO ND**	**16.0**	**620**	**49**	**4.86**	**0.25**	**Pt/FTO**

* (MSU-F-C ≈ ordered meso-cellular carbon foam)

2. **Sensitization of Photo anodes:**

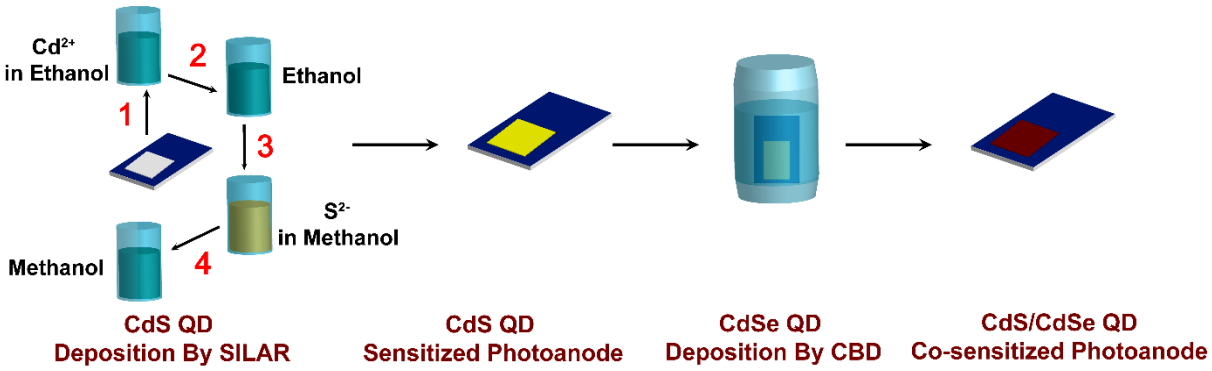

Figure S1: Sensitization of ZnO photoanodes with CdS and CdSe following Successive Ionic Layer Adsorption and Reaction (SILAR) and Chemical Bath Deposition (CBD) respectively.

3. Digital Photographs:

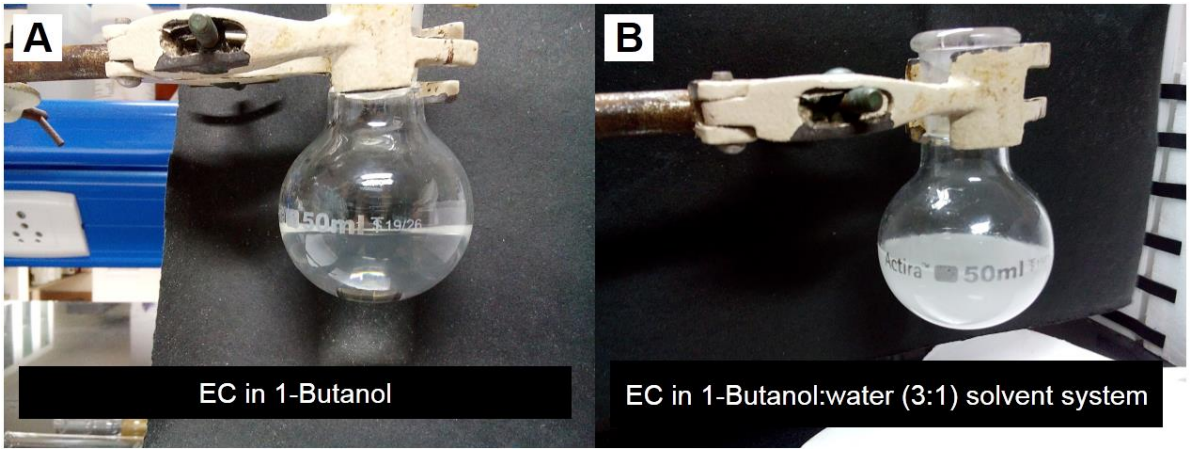

Figure S2: Digital photographs of solution of ethyl cellulose (EC) in **(A)** 1-Butanol and **(B)** 1-Butanol: Water (3:1) solvent system

4. Crystallite size calculations

The estimated the crystallite size of ZnO ND, ZnO NR, ZnO NS, CdS and CdSe NPs deposited onto the photoanodes by using Debye-Scherrer equation are shown in **table S2**.

The Debye-Scherrer equation is represented as:

$$D = \frac{0.94 \times \lambda}{\Delta W \times cos\theta}$$

Where, D is the crystallite domain diameter, λ is the wavelength of the incident X-ray beam (1.54 Å for the Cu Kα), θ is the Bragg's diffraction angle, ΔW the width of the X-ray pattern line at half peak-height in radians.

Table S2: Calculated crystallite size of the synthesized particles by using Debye-Scherrer equation

Name of the compound	Crystallite size (nm)
ZnO ND	~26.5
ZnO NR	~24.6
ZnO NS	~22.1
CdS NP	~5.3
CdSe NP	~5.1

5. Photoluminescence Analysis

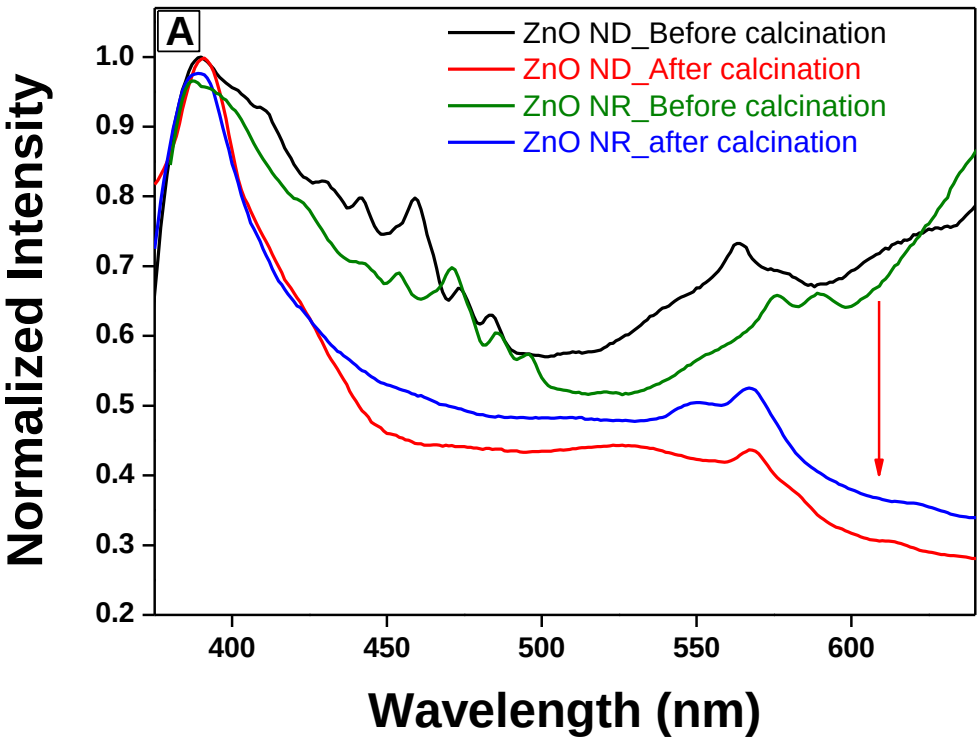

Figure S3: PL spectra of ZnO NDs and ZnO NRs before and after calcination

Figure S3 shows steady state PL spectra of ZnO NDs and ZnO NRs before and after calcination. After calcination, the near band edge emission peaks (~ 380 nm) for both the ZnO hetero-structures become sharper. In addition, the satellite peaks observed in the range of 420–500 nm originating from the co-ordinatively unsaturated Zn^{2+} interstitial sites (Zn_i, shallow donor) in the ZnO nanostructures are disappeared.[2] The intensity of broad emission bands in the visible region (~550-650 nm), attributed to the transition from the conduction band to the deep trap levels of ZnO (created by oxygen vacancies in the ZnO crystal structure), are observed to be reduced after calcination.[2, 3] Further we have fitted all the PL spectra in Gaussian mode and calculated the ratio of band edge emission peak intensity (I_b) to the defect level emission peak intensity (I_d) as shown in table S2:

Table S3: Ratio of band edge emission peak intensity (I_b) to the defect level emission peak intensity (I_d)

Name of the sample	I_b: I_d
ZnO ND before calcination	1.37
ZnO ND_after calcination	2.03
ZnO NR_before calcination	1.40
ZnO NR_after calcination	1.86

From table S3 we have observed that the values of I_b:I_d are increased for both the samples after calcination which implies the decrease in defect level emission and hence oxygen vacancies in ZnO crystal structure. All the aforementioned points are indicative of the reduction of intrinsic defect levels (both Zn_i and oxygen vacancies) of ZnO (ND and NR) hetero-structures after calcination.

6. Powder X-ray Diffraction Analysis

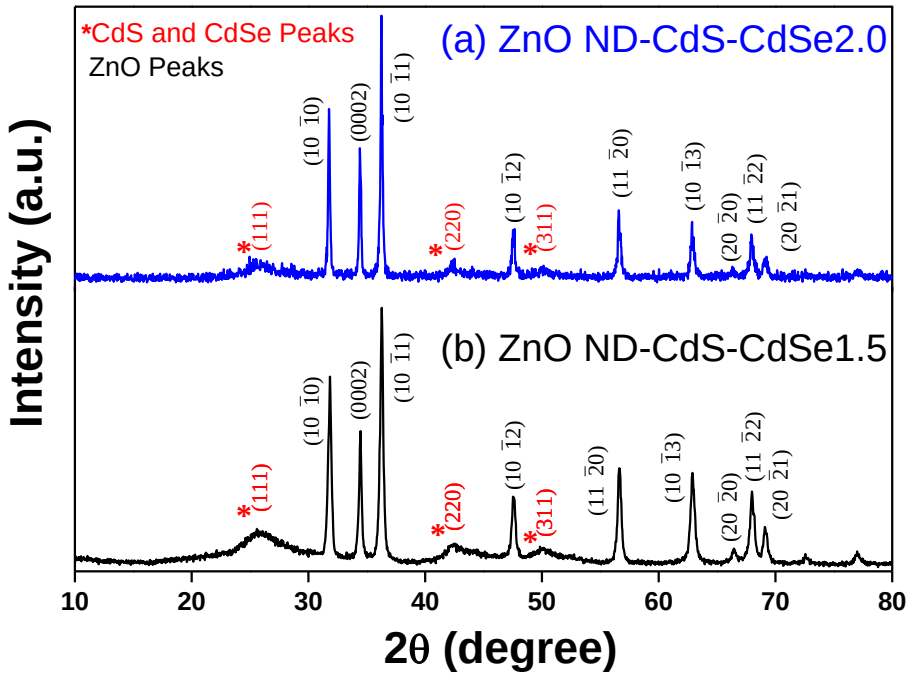

Figure S4: Powder X-ray Diffraction pattern for the photoanodes (a) ZnO ND-CdS-CdSe2.0 and (b) ZnO ND-CdS-CdSe1.5 respectively.

Figure S4 shows the PXRD pattern of ZnO ND-CdS-CdSe2.0 and ZnO ND-CdS-CdSe1.5. All the peaks are well indexed with hexagonal wurtzite phase ZnO (JCPDS Card No. 36-1451), cubic zinc blende CdSe (JCPDS no. 19-0191) and CdS (JCPDS no. 10-0454) with no detectable impurities.

Scheme S1. Schematic presentation of charge recombination in (a) ZnO ND-CdS-CdSe(2.0 mM) photoanode compared to the (b) ZnO ND-CdS-CdSe(1.5 mM) due to agglomeration of CdSe QDs.

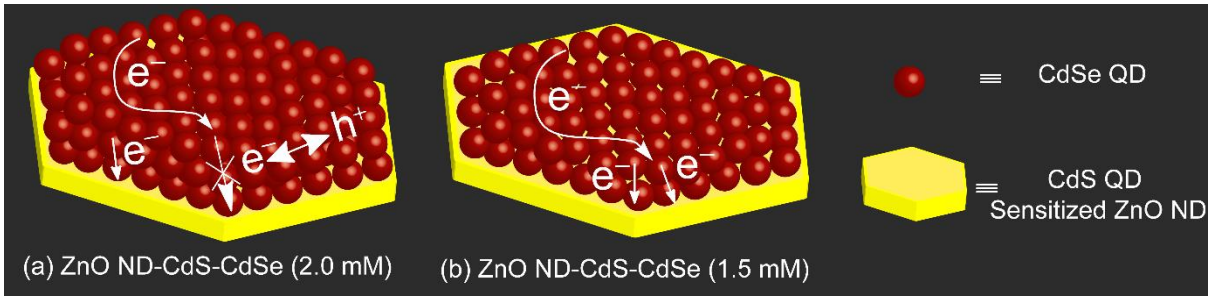

7. UV-Visible Absorbance analysis of the photoanodes

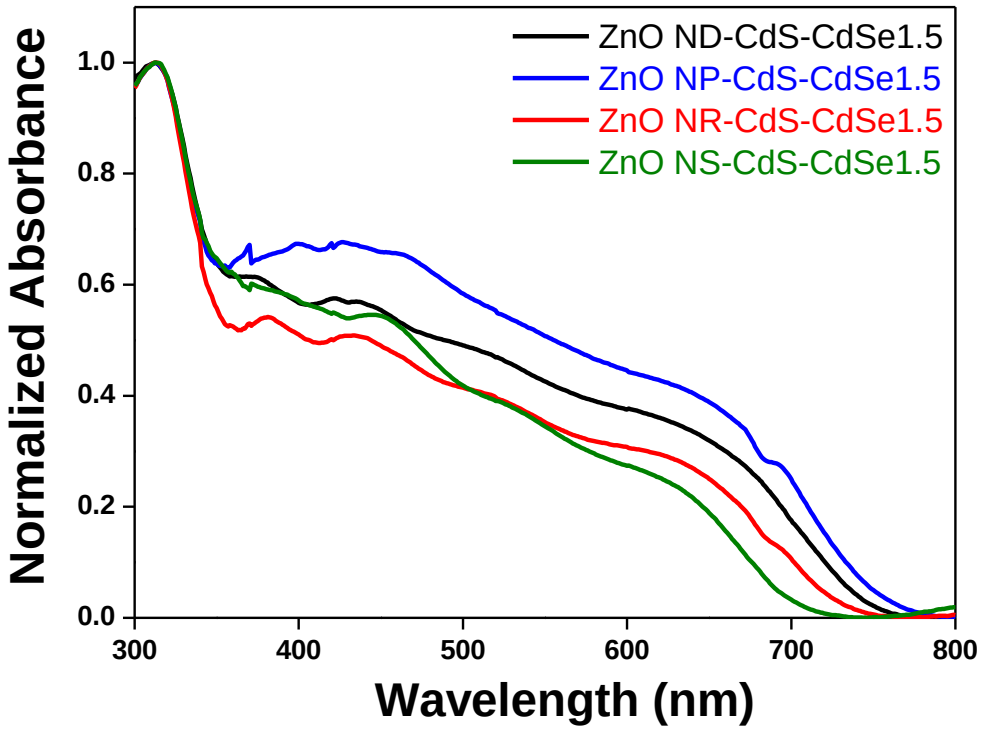

Figure S5: UV-Vis diffused reflectance spectra of CdS/CdSe co-sensitized ZnO ND, ZnO NP, ZnO NR and ZnO NS based photoanodes with 1.5 mM Se precursor concentration used during the chemical bath deposition (CBD) methods.

8. FESEM analysis of ZnO nanosheets:

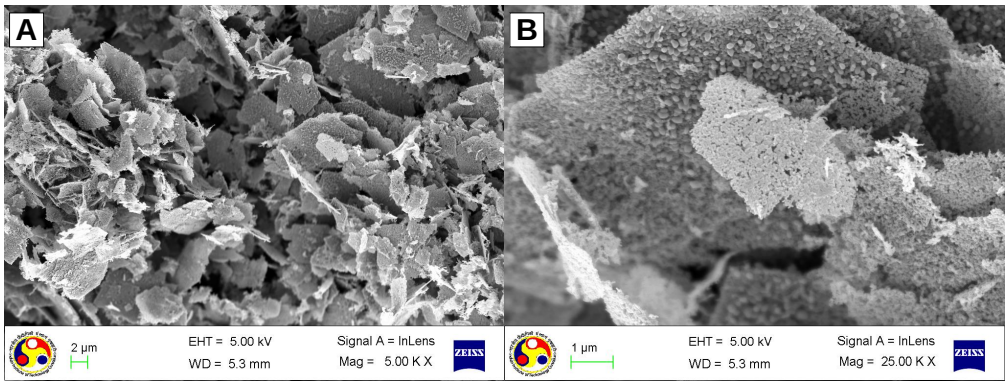

Figure S6: FESEM images of ZnO NSs showing layered structures at (A) lower and (B) higher magnifications

9. FESEM analysis of ZnO NDs showing lateral and longitudinal dimension:

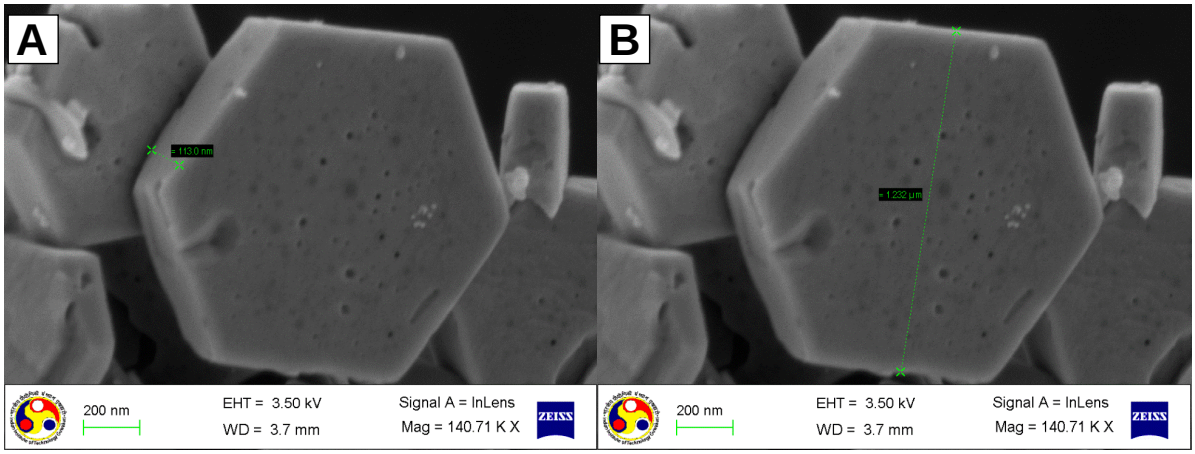

Figure S7: FESEM images of a ZnO NDs, (A) showing thickness is ~113 nm while its (B) longitudinal dimension is ~1.23 µm.

10. Estimation of average particle size of ZnO NDs by Dynamic Light Scattering (DLS) method

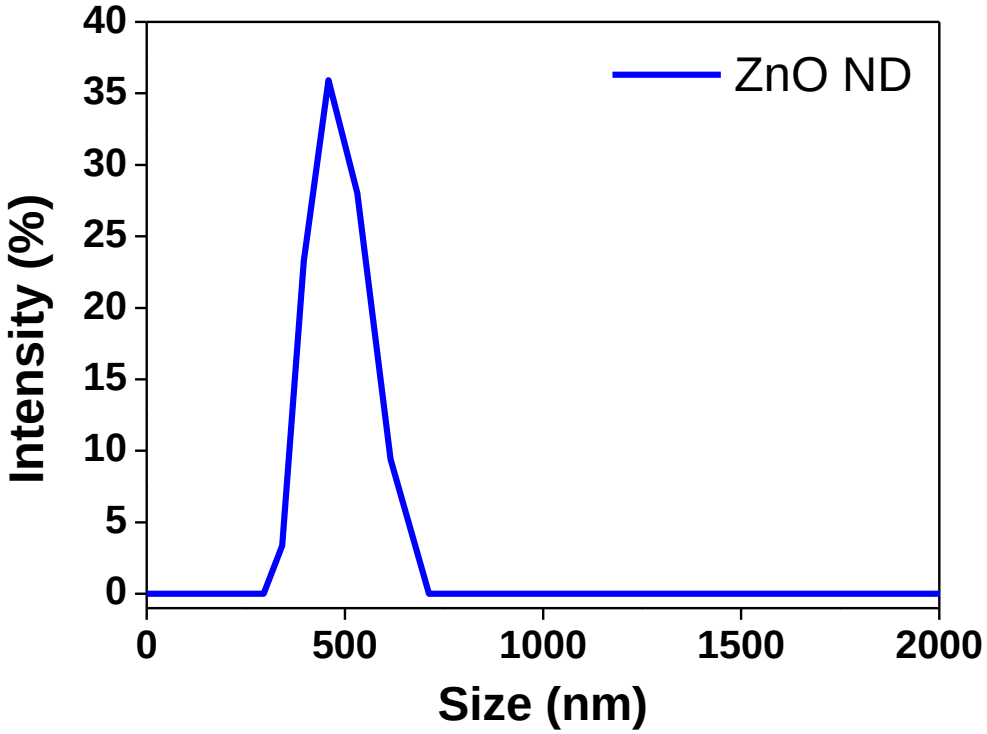

Figure S8: Size distribution plot for ZnO NDs in ethanol obtained from Dynamic Light Scattering (DLS) method.

In order to carry out Dynamic Light Scattering (DLS) method, we have dispersed ZnO ND in ethanol by ultra-sonication method for 1h and allowed to settle down for another an hour followed by size measurement with the help of a Malvern Zetasizer Nano ZS instrument. The size distribution of the particles are observed in the range of 400-550 nm as we have seen from figure R11. The deviation of size distribution is noted in DLS measurement as compared to the FESEM results are due to the hexagonal shape of ZnO NDs. It is well known that DLS technique is mainly used to measure the size of spherical particles in a solution.

REFERENCES:

(SI 1) Tian, J.; Zhang, Q.; Uchaker, E.; Gao, R.; Qu, X.; Zhang, S.; Cao, G. Architectured ZnO Photoelectrode For High Efficiency Quantum Dot Sensitized Solar Cells. *Energy Environ. Sci.* **2013**, *6*, 3542-3547.

(SI 2) Zeng, H.; Duan, G.; Li, Y.; Yang, S.; Xu, X.; Cai, W. Blue Luminescence of ZnO Nanoparticles Based on Non-Equilibrium Processes: Defect Origins and Emission Controls. *Adv. Funct. Mater.* **2010**, *20*, 561-572.

(SI 3) Wei, X. Q.; Man, B. Y.; Liu, M.; Xue, C. S.; Zhuang H. Z.; Yang, C. Blue Luminescent Centers and Microstructural Evaluation By XPS and Raman in ZnO Thin Films Annealed in Vacuum, N_2 and O_2. *Phys. B* **2007**, *388*, 145-152.